Spatial Oversampling for Robust LoS MIMO

Lalitha Giridhar, Maryam Eslami Rasekh, Ahmet Dundar Sezer, Upamanyu Madhow
Department of Electrical and Computer Engineering
University of California, Santa Barbara
Santa Barbara, California 93106
{lalitha, rasekh, adsezer, madhow}@ucsb.edu

***Abstract*—The combination of spatial multiplexing and large available bandwidths makes line-of-sight (LoS) multiple-input multiple-output (MIMO) in millimeter wave (mmWave) bands a particularly attractive approach for ultra high-speed wireless links. While standard LoS MIMO link designs require transceiver apertures matched to a nominal link range, along with careful alignment of transmit and receive antennas, in this paper, we investigate low-cost, opportunistically deployable LoS MIMO links, motivated by applications such as wireless backhaul in urban picocells. In such settings, geometric misalignment between transmit and receive arrays is inevitable, leading to multi-symbol delay spreads across the receive aperture. Furthermore, link ranges may vary significantly in such systems (e.g., from 50 to 150 meters in an urban backhaul), so that conventional LoS MIMO transceiver design, in which the array geometries are optimized to match a nominal range, is subject to potential collapse in the available spatial degrees of freedom (DoF) due to the sensitivity of the channel matrix to link and array geometries. For fixed transceiver apertures matched to a nominal range, we show that *spatial oversampling,* in which the number of receive antennas is increased beyond the number of spatially multiplexed data streams, provides robustness against both geometric misalignment and range variations. We demonstrate that the inter- and intra-stream interference resulting from misalignment can be suppressed effectively via spatially oversampled linear space-time equalization, where the equalizer complexity is controlled by adapting the time window of samples used for demodulation across data streams and receive antennas. We also show that spatial oversampling alleviates potential DoF collapse, quantified here as the noise enhancement of a zero-forcing equalizer, from link range variations. Our numerical results are for parameters corresponding to a concept system with data rate 128 Gbps at a nominal link range of 100 m, using 4 spatially multiplexed streams at a carrier frequency of 130 GHz.**

***Index Terms*—mmWave, LoS MIMO, space-time equalization, adaptive, spatial oversampling, interference vectors, LMMSE signal recovery, mode collapse, spatial correlation, ZF equalization, noise enhancement**

I. Introduction

The high data rates offered by millimeter wave (mmWave) line-of-Sight (LoS) multiple-input multiple-output (MIMO) communication systems have generated significant recent interest [1]–[3]. The available spatial degrees of freedom (DoF) for a LoS MIMO link with two-dimensional (2D) transmit and receive arrays having areas A_T and A_R respectively, and separated by a link distance R is given by [4], [5]

$$DoF_{\text{2D}} \approx \frac{A_T A_R}{R^2 \lambda^2} + 1 \tag{1}$$

Since the available spatial DoF scales inversely with the square of the carrier wavelength λ, the scaling with the carrier frequency $f_c = c/\lambda$ (c denotes the speed of light) is quadratic. Since the transmission bandwidth typically also scales linearly with carrier frequency, the overall data rates offered by LoS MIMO links can potentially scale as f_c^3. Furthermore, (1) also indicates that the required antenna apertures for a given DoF scale as λR for a 2D array, corresponding to a spacing between neighboring antennas scaling as $\sqrt{\lambda R}$. Thus, smaller apertures corresponding to more compact transceiver form factors, can be employed as the carrier frequency increases. Exploration of LoS MIMO for high-frequency mmWave and terahertz (THz) bands is motivated by these attractive scaling properties. Advances in silicon RFICs beyond 100 GHz [6] open up the possibility for low-cost, compact transceivers which can be opportunistically deployed (e.g., for picocellular wireless backhaul). However, the current paradigm of LoS MIMO links must be rethought in order to realize this potential: flexible deployment means endemic misalignment, and that the transceiver geometry (designed for a nominal link range) is not necessarily matched to the actual link range. In this paper, we show that spatial oversampling at the receiver can be used to overcome both of these difficulties.

LoS MIMO with critical spatial sampling: The DoF promised by (1) can be attained by setting the transmit and receive antennas equal to the number N of multiplexed data streams. We term this approach *critical spatial sampling,* since the number of receive antennas is the minimum needed for linear separation of the N multiplexed streams. Consider a symmetric design with equal 2D transmit and receive apertures, and $N = n^2$ antennas at each end, spaced in a uniform 2D grid. In this case, the Rayleigh spacing between adjacent antenna elements, which ensures that the receive array responses due to different transmitted data streams are orthogonal, is given by [4], [5]

$$d = \sqrt{\lambda R/n} \tag{2}$$

For a link range of $R = 100$ m, a standard 4×4 LoS MIMO ($N = 4$, $n = 2$) design at a carrier frequency of 130 GHz corresponds to an antenna spacing of $d = 34$

This work was supported in part by CUbiC (and earlier by ComSenTer), one of six centers in JUMP, a Semiconductor Research Corporation (SRC) program sponsored by DARPA.

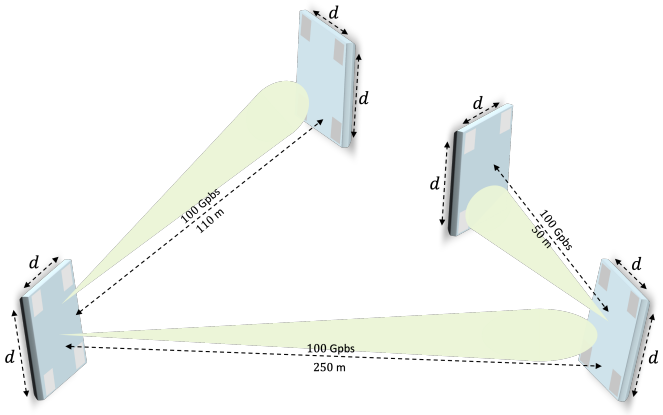

Fig. 1. Example deployment scenario where misalignment of panels and varying link ranges of operation is an inevitable consequence

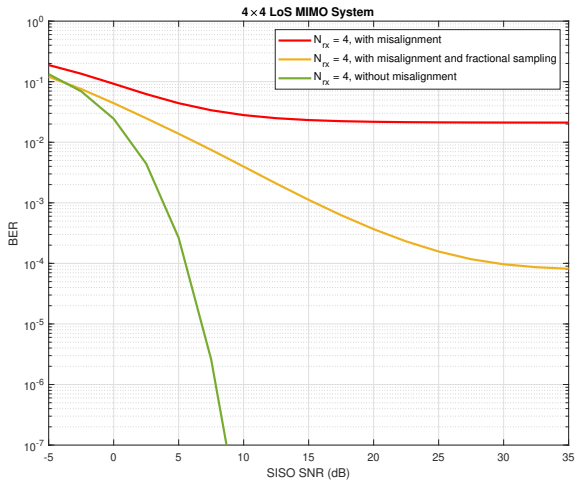

Fig. 2. Impact of misalignment in a 4×4 LoS MIMO system

cm, and data rates in excess of 100 Gbps are attainable, for example, using 25 GHz bandwidth and Quadrature Phase Shift Keying (QPSK) modulation, even after allowing for a excess bandwidth factor and lightweight channel coding. This combination of compact form factors (e.g., enabling opportunistic deployment on lamp posts) and high data rates is particularly attractive for the relatively short-range links required for urban wireless backhaul networks as depicted in Fig. 1. However, as we discuss below, critically sampled LoS MIMO is not robust enough to provide the flexibility required for opportunistic deployment, leading to our proposed approach of spatial oversampling where additional receive antennas are placed within the given aperture without increasing the required form factor.

The impact of geometric misalignment: Opportunistically deployed LoS MIMO must contend with the channel dispersion caused by geometric misalignments between the transmit and receive arrays. For example, even a small vertical misalignment with a tilt angle of 7.5° degrees at 20 Gbaud causes a 6 symbol channel delay spread across the receive aperture, leading to inter-symbol interference (ISI) within and between the multiplexed data streams. Fig 2 demonstrates the effect of geometric misalignment on a ideal 4×4 LoS MIMO system with singlecarrier modulation. Error floors appear in the bit error rate curve even with a small misalignment. The figure also shows that error floors persist even when we apply fractionally-spaced equalization using $T/2$-spaced sampling points. While fractionally spaced sampling suffices for temporal channel inversion in SISO systems [7], [8], it does not provide enough degrees of freedom to overcome spatial interference across streams. Moreover, the challenge of analog-to-digital conversion at high sampling rates renders the temporal oversampling required for fractionally spaced equalization unattractive. We therefore focus on symbol rate sampling for this study, and show that spatial oversampling provides the degrees of freedom required to avoid incurring error floors.

The impact of link range variations: For ideal LoS MIMO with critical spatial sampling matched to a nominal link range, the spatial DoF could collapse at specific ranges even smaller than the nominal range [5]. Our investigation shows that this phenomenon of mode collapse for fixed transceiver form factor persists for misaligned LoS MIMO with critical sampling as well. Clearly, for flexibility of deployment, we would like to reduce such sensitivity to link range variations. We show that spatial oversampling provides robustness against such variations.

Contributions: Our main contributions are summarized as follows:

(i) We propose and investigate *spatial oversampling* as a means of providing robustness against both geometric misalignment and link range variations. For our concept system with 4 spatially multiplexed streams at 100 m nominal range, the overall area of the receive array including the original set of 4 receive elements is approximately $147^2\lambda^2$ to satisfy the required spatial degrees of freedom. Additional receive elements (beyond the number of transmit streams) can therefore be easily integrated into the receive array within this available form factor.

(ii) We show that spatial oversampling is effective for combating the dispersion due to geometric misalignment while maintaining symbol rate sampling. The linear space-time equalizer for each data stream uses a possibly different time window of samples at each receive antenna, adapted to the relative delays seen by the stream at different receive antennas. This coarsely aligns the received signals in time, reducing the complexity of space-time equalization. We show that linear space-time equalizers of reasonable complexity, designed by employing a suitable combination of spatial oversampling and adaptive time windowing, eliminate the error floors caused by geometric misalignment.

(iii) We illustrate that mode collapse due to link range variations is greatly alleviated by spatial oversampling. We quantify this phenomenon by studying the variation in

noise enhancement for zero-forcing space-time equalization as a function of link range. The impact of receive element geometry on the array aperture is also explored and it is shown that by intelligently picking the receive geometry, mode collapse can be circumvented at a given link range by using a smaller spatial oversampling factor.

We focus on singlecarrier modulation with relatively small constellations in our modeling and evaluation, since these pose moderate requirements on dynamic range (which is a challenge at high carrier frequencies and large bandwidths) compared to OFDM. However, our observations on the benefits of spatial oversampling are broadly applicable to a variety of time-frequency signal designs.

As an important aside regarding the feasibility of our concept system of 4×4 LoS MIMO at 130 GHz, we note that the link budget for the envisioned system is easily attainable with emerging low-cost CMOS radio frequency integrated circuits (RFICs) in the upper mmWave bands and is illustrated in Appendix A.

II. Related Work

Current LoS MIMO systems launched by industry (such as [9], which employs a 2.5 GHz bandwidth in E-band $(70 - 80$ GHz carrier frequency$)$ require bulky antenna structures and highly skilled installation. We focus on higher frequencies and shorter ranges, targeting transceivers with compact form factors that do not require expert installation. For opportunistic deployment in applications such as urban picocellular fronthaul, midhaul and backhaul, ensuring robustness to geometric misalignment of transceiver panels and link range variations is critical for reliable operation.

While the impact of geometric misalignment in LoS MIMO systems is a topic of growing interest [10]–[13], to the best of our knowledge, the proposed combination of spatial oversampling combined with adaptive time windowing has not been explored previously. In [10], for 2×2 single-polarized and 4×4 dual-polarized LoS MIMO, various training-based algorithms and blind algorithms for equalization are analyzed. The simulation results provided for the considered LoS MIMO systems operating at a carrier frequency of 19 GHz and symbol rate of 50 MHz indicate the need for complex space-time equalizers with time windows of more than 40 symbols in order to handle the frequency selectivity of the channel. A sequential channel equalization method for LoS MIMO, where the channel is factorized into a product of three matrices with the middle one dominated by an inverse discrete Fourier transform (DFT) matrix, is considered in [11]. The equalization is subsequently performed in the reverse order of factorization. Our setting differs as the operating bandwidths are much larger (10s of GHz), causing multi-symbol delay spread even for small misalignment angles. This symbol level dispersion is not taken into account in [11]. In addition, by employing the adaptive time-windowing strategy along with spatial oversampling, the space-time equalizer complexity is reduced significantly in comparison to [10]. The use of spatial oversampling to overcome sub-symbol delays was shown in [13], which is closest to our current work. However, the model considered in [13] assumes random delays at each receive antenna, whereas in this work, a more realistic delay spread model based on the specific system geometry corresponding to the misalignment angles and array size is considered. Moreover, our work provides far more detailed insight into the signal space considerations for avoiding error floors with linear equalization, highlighting the trade off between the number of additional receive antennas and the temporal window size used for equalization.

The optimal antenna spacing at a particular carrier frequency for standard LoS MIMO link designs with transceiver apertures matched to a nominal link range of operation is well studied [5], [14]. The use of non-uniform array structures to overcome mode collapse as a result of operating at non-optimal link ranges is explored in [15]–[18]. In [17], a uniform cross array is proposed to ensure stable and high channel capacity for a LoS transmission feeder link which involves communication between a ground station and a high altitude platform station (HAPS) which is subject to degradation in the channel capacity due to movement of the HAPS causing changes in the distance and angle. The work in [18] discusses optimized non-uniform antenna array structures for autonomous unmanned aerial vehicles (UAV) based LoS MIMO transmission. While using non-uniform arrays has been proven to be an effective solution to enhance robustness to link range variations, our work focuses on using regular array geometries for spatial oversampling within the available aperture to combat mode collapse while operating at ranges different from the nominal. For example, while a standard 4×4 LoS MIMO link designed for 100 m suffers mode collapse at 50 m, 3X spatial oversampling within the same receive aperture can be designed to prevent mode collapse at link ranges down to 10 m. In [19], it is shown that by utilizing a general expression for the optimum antenna separation product (ASP) which consists of multiple solutions, robustness to a subset of certain link range values between 10-100 m can be obtained for a given inter-antenna spacing. This is achieved by picking the solution to the ASP equation that does not necessarily correspond to the smallest inter-antenna separation (and hence the most compact form factor) for a given link range.

This paper builds on our preliminary results presented in a conference paper [20], in which the use of spatial oversampling combined with adaptive time windowing was shown to be an effective strategy to combat the effects of geometric misalignment between transceiver panels in LoS MIMO systems. The present paper goes significantly beyond [20] in two key aspects. While [20] assumed explicit channel knowledge at the receiver, in the present paper, we consider an MMSE space-time equalizer adapted based on a training sequence. In addition, we investigate the use of spatial oversampling to enhance robustness to link range variations.

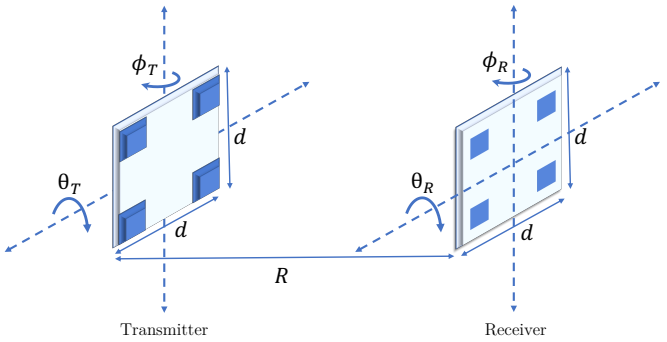

Fig. 3. Geometric misalignment configuration for the 4×4 LoS MIMO system

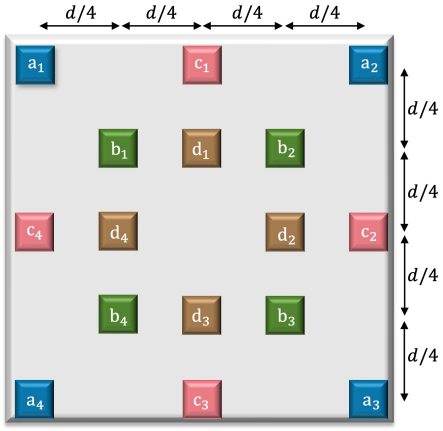

Fig. 4. Geometry of additional receive elements in groups of four within the same form factor

III. System Model

Consider a 25 GHz bandwidth LoS MIMO system with N_{TX} transmit and N_{RX} receive antennas at a link distance of R_o operating at a carrier frequency of $f_c = 130$ GHz. As shown in Fig. 3, we assume $N_{\text{TX}} = 4$ transmitters placed at the four corners of a $d = 34$ cm sided square aperture separated by $R_o = 100$ m from the $N_{\text{RX}} \geq 4$-element receiver of the same aperture for our running example. Symbol rate sampling is assumed with a symbol duration of $T_s = 50$ ps and per stream symbol rate of $1/T_s = 20$ Gigabaud. Each of the four transmit antennas independently transmit symbols drawn from the QPSK alphabet with linear MIMO reception at the receiver. We can characterize the impulse response of the channel between the transmitter m and receiver n as

$$h_{nm}(t) = \delta(t - \tau_{nm}). \tag{3}$$

where τ_{nm} is the time of flight, which varies across (m, n) due to geometric misalignment. The QPSK data streams are pulse shaped using a raised cosine pulse train filter with a roll-off factor $\beta = 0.25$. At the receiver, the energy of each symbol spreads across the time domain over multiple samples due to ADC sampling times not being aligned with the peak of the pulse shaping waveform. We therefore consider a window of $L_P = 5$ samples for each pulse, which captures most (about 99%) of the pulse energy. The discretized signal at the ADC output of receiver n at time $kT_s = k$ is then described by

$$y_n[k] = \sum_{m=1}^{N_{\text{TX}}} \sum_{l=-(L_p-1)/2}^{(L_p-1)/2} e^{-j2\pi f_c \tau_{nm}} s_m[k - \bar{\tau}_{nm} + l] \; p(\tilde{\tau}_{nm} - l) + w_m[k] \tag{4}$$

where $s_m[k]$ denotes the unit-amplitude QPSK symbol transmitted from antenna m at discrete time k ($|s_m[k]| = 1$), $w_m[k] \sim \mathcal{CN}(0, \sigma^2)$ are the i.i.d. additive complex Gaussian noise terms, and $p(t)$ is the raised cosine pulse function evaluated at a time offset t.

The elevation and azimuth rotations of the transmit array are denoted by θ_{T} and ϕ_{T}, respectively. In a similar fashion, for the receive array, the elevation and azimuth rotation angles are denoted by θ_{R} and ϕ_{R} as shown in Fig. 3. When there is no misalignment of the transmit and receive panels, i.e., when the antennas face each other, the small path length differences between the transmitter-receiver pairs result in only sub-symbol-period delays. However, even a slight misalignment of either panel can cause delay spread across the aperture, necessitating space-time equalization for accurate decoding. In order to model this geometric misalignment of the panels we consider rotations drawn randomly within the range of $[-7.5°, 7.5°]$ degrees, which result in up to a 6-symbol delay offset across the receive aperture.

Spatial oversampling for Geometric Misalignment: We consider symbol rate sampling with spatial oversampling to furnish the necessary dimensions for effective space-time interference suppression. We consider different factors of spatial oversampling in our system ranging from 1 (no oversampling) to 4 which then corresponds to the number of receivers varying between 4 and 16 respectively in groups of four. Fig. 4 shows the placement of these additional receive antenna groups labeled from 'a' to 'd' on the receive aperture. In order to achieve an adequate link budget, each "receiver" can be implemented either as a fixed beam directive antenna or as a sub-wavelength spaced subarray employing electronic beamsteering, such as RF beamforming directed towards the transmitter.

Motivation for Adaptive windowing: For the range of misalignments considered in our numerical examples, aggregating the effect of temporal pulse spread (due to off-peak sampling) and delay variation (due to platform tilt), the maximum spread in terms of samples for any given symbol across the receive array is at most equal to $t_{\text{spread}} = 5 + 6 = 11$. A naive space-time equalizer that employs a fixed window of time domain samples across all receive elements to make a decision on a given symbol would therefore need to employ a time window of 11 samples, leading to excessive complexity with increase in the number of receive elements. As we discuss in the next section, adaptive windowing together with spatial oversampling sidesteps this difficulty, leading to substantial savings in computation.

Spatial Oversampling for Varying Link Ranges: For the targeted deployment scenarios (e.g., wireless fron-

thaul/midhaul/backhaul in urban picocells), robustness to link range variations is critical. For our concept system at $f_c = 130$ GHz, we set the nominal link range to $R_o = 100$ m as a typical value in a dense urban environment. Even with ideal alignment, DoF collapse can happen as the operating link range varies from R_o, and misalignment does not help. We show that spatial oversampling alleviates mode collapse, using design guidance (choosing the number and locations of receive elements from Fig. 4) based on a single metric that is easy to compute: the noise enhancement of a Zero-Forcing (ZF) equalizer for an ideally aligned system. The designs are shown to work for both ideally aligned and misaligned systems, as long as the latter uses a suitable adaptive space-time equalizer.

IV. Adaptive Space-Time Equalization

In this section, we describe adaptively-windowed space-time equalization for misaligned LoS MIMO. We consider the following example for concrete illustration of our design approach: 4×8 LoS MIMO (i.e., spatial oversampling factor of 2) with misalignment angles between the transmit and receive arrays given by: $\theta_{\mathrm{T}} = 3.67°$, $\phi_{\mathrm{T}} = -4.30°$, $\theta_{\mathrm{R}} = 6.36°$, and $\phi_{\mathrm{R}} = 7.19°$. (These were randomly generated.)

Consider a "desired symbol" $x_1[k]$ transmitted from transmit antenna 1 that we wish to demodulate. As indicated by the black-colored pulses in Fig. 5, the time of arrival of this desired symbol at each receiver is different due to the different link distances between the transmit antenna 1 and the 8 receive antennas. The fainter pulses shown in Fig. 5 are the receive responses corresponding to past and future symbols emitted by transmit antenna 1 and the integer values on the x-axis correspond to the sampling points of the ADC at each receive antenna.

Since the peak response of the desired symbol $x_1[k]$ corresponds to a different time index at different receive antennas, each receiver adapts its window of samples to align with the peak response from $x_1[k]$ at that antenna. From Fig. 5, we infer that the considered misalignment causes up to 5-symbol delay offsets across the receive aperture, and a time window of size $W = 3$ has been employed at each receive antenna to align with the peak response of the desired symbol. Note that the time window at each receive antenna can, in principle, be adapted for each pair of transmit and receive elements.

The strategy behind the choice of the window size W is based on the twin goals of capturing enough energy from the desired symbol and providing sufficiently high signal space dimension for space-time interference suppression. The choice of $W = 3$ suffices to capture about 95% of the energy of the desired symbol for the raised cosine pulse considered. The length of the resulting space-time equalizer would then be WN_{RX}. It is important to ensure that this length provides a large enough "signal space" dimension such that linear interference suppression suffices for handling ISI due to past and future symbols from the transmit antenna emitting the desired symbol as well as the impact of cross-stream interference (CSI) due to symbols emitted by the other transmit antennas. Keeping in mind this complexity trade-off,

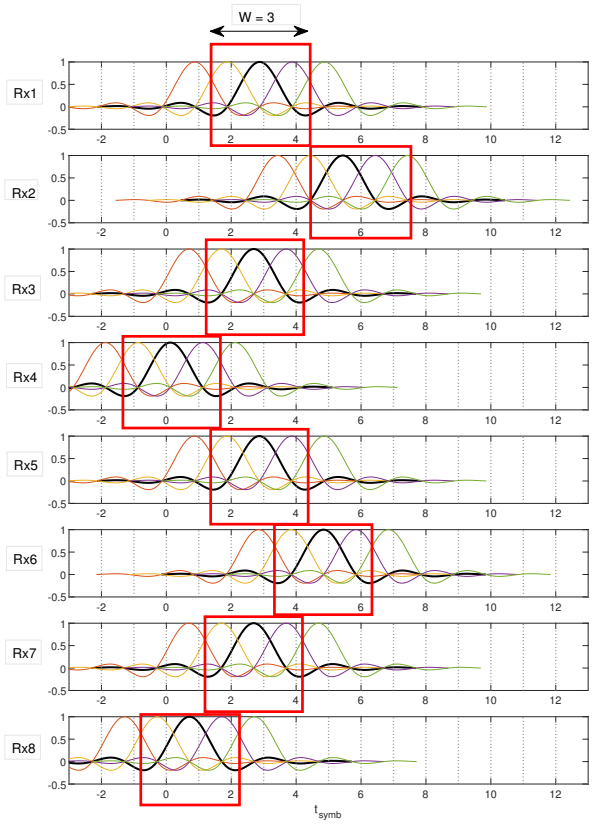

Fig. 5. Adaptive window, $W = 3$ described across $N_{RX} = 8$ receivers

one might choose a larger window if the number of receive antennas is small, or a smaller window if the number of receive antennas is large. However, for fixed WN_{RX}, different choices of W and N_{RX} lead to signal space geometries corresponding to different interference suppression capabilities.

In order to demodulate a given symbol from a given stream, say $x_1[k]$, the kth symbol from stream 1, each receiver employs an adaptive time window, collecting the W ADC samples with the maximum contribution from $x_1[k]$. Collecting these samples from the different receivers, we obtain a vector of length $N_{RX}W$. The space-time equalizer for stream 1 operates on this vector to obtain a decision statistic for $x_1[k]$. While W can be varied across transmit-receive pairs to meet the twin goals of capturing enough energy from the desired symbol and providing a signal space geometry that permits effective interference suppression, we find that our choice of considering a fixed window size W across all transmitter-receiver pairs (Figure 5), adapted to capture signal energy in Figure 5, provides excellent performance.

Even though we consider a Nyquist raised cosine pulse and no channel dispersion, since we employ a fixed clock common to all receivers, geometric misalignment implies that the sampling times are, with probability one, not aligned with the peak of the raised cosine pulse at any of the receivers, which results in intersymbol interference (ISI) For example, in Figure 5 the output of receive antenna $\#4$ at time k has contribution from other previous and next symbols in the

sequence as well as the main contribution from the desired symbol at time k. Geometric misalignment also implies that the received space-time responses for different streams are no longer orthogonal, resulting in cross-stream interference (CSI).[1]

We can count the number of ISI and CSI symbols falling into the space-time window selected to demodulate the desired symbol in our example as follows:

- A given symbol spans L_P samples (e.g., we may set $L_P = 5$ for the raised cosine pulse). A spread of $L = L_P + W - 1$ symbols from each antenna stream thus have non-negligible contribution to the samples in the observation window of size W. It is important to note that since we choose the window at each receive antenna to align around the peak response to the desired symbol transmitted from transmit antenna $\#1$, the *same* set of ISI and CSI symbols fall into the chosen window for all receivers.
- Given W and L_P, the number of ISI symbols falling into the chosen window can be found from $L_P + W - 2 = L-1$. For our running example with $L_P = 5$ and $W = 3$, the number of ISI symbols is then equal to 6.
- The number of CSI symbols falling into the window of size W is $L(N_{\text{TX}} - 1)$ which for our example equals 21.
- The total number of interfering symbols (ISI + CSI) falling into the space-time window used to demodulate a desired symbol is then given by $LN_{\text{TX}} - 1$ and is equal to 27 symbols for the considered example.

The vector response to each such interfering symbol within the space-time window is called an interference vector, while the vector response to the desired symbol is called the desired signal vector. The goal of linear space-time equalization is to suppress the interference vectors without incurring excessive noise enhancement. The dimension of the signal space in which we are operating is the length of the space-time equalizer and can be given as WN_{RX}.

The preceding model is concisely represented by defining the channel H_s that produces the windowed observation vector for a desired symbol from stream s as:

$$\begin{aligned}(\mathbf{y}_s)_{N_{\text{RX}}W\times 1} &= (\mathbf{H}_s)_{N_{\text{RX}}W\times N_{\text{TX}}L}\,(\mathbf{x}_s)_{N_{\text{TX}}L\times 1} \\ &= [\mathbf{h}_{s,1} \quad \mathbf{H}_{s,\text{ISI}} \quad \mathbf{H}_{s,\text{CSI}}] \begin{bmatrix} x_1 \\ \mathbf{x}_{\text{ISI}} \\ \mathbf{x}_{\text{CSI}} \end{bmatrix}, \quad (5)\end{aligned}$$

where $\mathbf{h}_{s,1}$ is the $N_{\text{RX}}W \times 1$ response of the desired symbol x_1 on the window, $\mathbf{H}_{s,\text{ISI}}$ is the $N_{\text{RX}}W \times (L-1)$ channel response of the $L-1$ ISI terms $\mathbf{x}_{\text{ISI}}$, and $\mathbf{H}_{s,\text{CSI}}$ is the $N_{\text{RX}}W \times (N_{\text{TX}}-1)L$ channel response of the $L-1$ CSI terms $\mathbf{x}_{\text{CSI}}$ on the observation window.

At high SNR, the linear Minimum Mean Squared Error (MMSE) equalization tends to the linear zero-forcing (ZF) equalizer, assuming that the zero-forcing equalizer, which projects the received vector orthogonal to the subspace spanned by the interference vectors, exists. Since we wish to operate at relatively high SNRs without incurring error floors, we target regimes in which the ZF equalizer does exist. Assuming linearly independent interference vectors (a worst-case assumption maximizing the dimension of the interference subspace which is usually satisfied), a necessary condition (which is often also sufficient) for the existence of the ZF equalizer is that the dimension of the signal space should be higher than the number of interference vectors. We can now obtain simple design rules to predict whether linear interference suppression will work well, by counting the number of interference vectors, and comparing it with the length of the space-time equalizer.

[1]We hope that, given the very different context, the use of an acronym commonly employed for channel state information will not cause confusion.

TABLE I
NUMBER OF INTERFERENCE VECTORS AND THE DIMENSION OF THE SIGNAL SPACE FOR DIFFERENT W WHEN $L_P = 5$ PER STREAM

W	**Interference Vectors**	**Dimension of Signal Space**				
		$N_{\text{RX}} = 4$	$N_{\text{RX}} = 6$	$N_{\text{RX}} = 8$	$N_{\text{RX}} = 12$	$N_{\text{RX}} = 16$
1	19	4	6	8	12	16
3	27	12	18	24	36	48
5	35	20	30	40	60	80

We calculate and tabulate in Table I the number of interference vectors and the corresponding dimension of the signal space, for different W values, varying the spatial oversampling factor between 1 and 4. For 4×4 LoS MIMO without oversampling, it can be seen from Table I that the dimension of the signal space is less than the number of interference vectors for all window sizes considered ($W \in \{1, 3, 5\}$). Thus, linear space-time equalization is expected to perform poorly without spatial oversampling. On the other hand, for a 4×8 system (i.e., 2X spatial oversampling) with a window of size $W = 5$, the signal space dimension clearly exceeds the number of interfering vectors, so that the LMMSE receiver is expected to perform well. It is important to recognize that in some cases where the signal space dimension is less than the number of interference vectors, the LMMSE receiver may still perform adequately, since some of the interference vectors could be relatively weak, and the residual interference due to the inability to completely suppress them is small enough to avoid discernible error floors at the SNRs of interest (and for the small constellations considered).

A. Adaptive Channel Equalization: We consider a block least squares implementation for the adaptive LMMSE receiver, which is calculated separately for each stream $s \in \{1, \ldots, N_{TX}\}$ based on that stream's adapted window. For L training symbols for each stream (we use $L = 250$ randomly drawn QPSK symbols for each stream in our numerical results), the $WN_{\text{RX}} \times 1$ LMMSE equalizer for stream s is given by [21]

$$\mathbf{c_s} = \mathbf{R^{-1}p_s} \quad (6)$$

where $\mathbf{R}$ with dimension $WN_{RX} \times WN_{RX}$ and $\mathbf{p_s}$ of size $WN_{RX} \times 1$ are calculated by taking empirical averages over

the block of L received vectors $\mathbf{y}_l$ as

$$\mathbf{R} = \frac{1}{L}\sum_{l=1}^{L}\mathbf{y}_l(\mathbf{y}_l)^H \tag{7}$$

and,

$$\mathbf{p}_s = \frac{1}{L}\sum_{l=1}^{L} b^*[l-\Delta_s]\mathbf{y}_l \tag{8}$$

where, Δ_s is the decoding delay per stream s and is equal to $(W+1)/2$ where W is the adaptive time-window employed for that stream. Thus, we computeN_{TX} LMMSE receivers, one for each transmitted stream.

After the training phase, the decision statistic for a given symbol of stream s is given by the linear correlator output:

$$\hat{x}_s = \mathbf{c}_s^{\mathbf{H}}\mathbf{y}_s \tag{9}$$

where $\mathbf{y}_s$ is the vectorized representation of the received signal window for that symbol.

In order to evaluate the performance of the adaptively windowed misaligned LoS MIMO system for various window sizes and spatial oversampling factors, we consider two performance metrics: i) average per-stream bit error rate (BER), and (ii) ratio of SINR to nominal (ideal) beamformed SNR. The nominal beamformed SNR, denoted by SNR_{bf}, is

$$\text{SNR}_{\text{bf}} = \frac{N_{\text{RX}}}{\sigma^2}$$

based on the assumption of unit amplitude (average) channel gains and unit energy transmit symbols. Note that the SNR_{bf} is a factor N_{RX} higher than the SISO SNR. The SINR of stream s is evaluated based on our extended channel model and the output of the LMMSE receiver as follows:

$$\text{SINR}_s = \frac{|\mathbf{c}_s^H\mathbf{H}_s\boldsymbol{\delta}_1|^2}{\sum_{\substack{i\in\Gamma_s\\ i\neq 1}}|\mathbf{c}_s^H\mathbf{H}_s\boldsymbol{\delta}_i|^2+\sigma^2|\mathbf{c}_s^H\mathbf{c}_s|^2} \tag{10}$$

where $\boldsymbol{\delta}_i$ is a $|\Gamma_s|$-long input vector with "1" on index i and zeros everywhere else. Based on our convention, note that the index "1" corresponds to the desired symbol or signal vector of stream s that is falling into the adaptive window for that stream.

We average our results over 10^3 misaligned link realizations, where each realization has random horizontal and vertical tilts at the transmitter and receiver, drawn uniformly from $[-7.5°, 7.5°]$ for the nominal system model described in Section III. From our interference vector counting analysis, it is expected that for system realizations with insufficient spatial oversampling and/or window size, we should see BER floors at high SNRs due to the lack of sufficient dimensionality for full interference suppression.

Fig. 6 plots the BER curves for different oversampling rates corresponding to $N_{\text{RX}} = 4, 8, 12$ and 16 and window sizes $W = 1, 3, 5$. As expected, without any spatial oversampling ($N_{\text{RX}} = 4$), there are error floors even with larger window sizes. With spatial oversampling, however,error floors are avoided even with a relatively small window size W. As the spatial oversampling factor increases, smaller window sizes suffice for avoiding error floors. The observations from Fig. 6, for the most part, are consistent with the interferer counting arguments summarized in Table I. An apparent exception is $N_{\text{RX}} = 8$ and $W = 3$, for which there are no discernible error floors in Fig. 6, despite the signal space dimension being smaller than the number of interference vectors in Table I. However, the additional interferers appear at the peripheries of the time window, corresponding to severely attenuated tails of the raised cosine pulse. Thus, the adaptive LMMSE receiver does not need to "expend signal space dimension" for suppressing these interference vectors. While the residual interference is too small to impact the BER plot for QPSK signaling, the SINR to SNR gap can be more informative regarding its size.

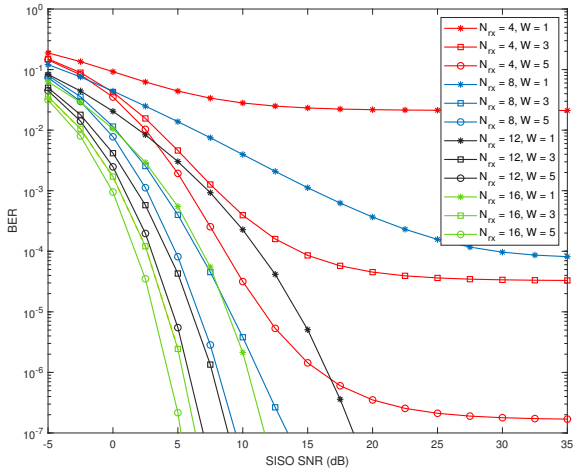

Fig. 6. Bit error rate versus SISO SNR for different values of N_{RX} and W.

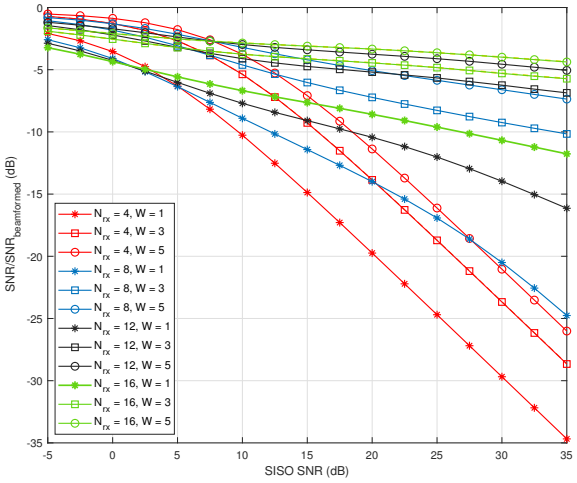

Fig. 7. SINR to beamformed SNR ratio versus SISO SNR for different values of N_{RX} and W

The SINR to beamformed SNR ratio of the different cases is plotted in Fig. 7. In cases where the full interference

TABLE II
OPTIMAL ELEMENT SPACING FOR VARYING LINK RANGE VALUE FOR A 4×4 LOS MIMO SYSTEM OPERATING AT 130 GHZ

R (m)	25	50	100	150
d (cm)	0.17	0.23	0.34	0.42

suppression/zero forcing is not possible due to the lack of dimensionality, this gap grows arbitrarily large. With sufficient dimensionality however, the noise enhancement from the zero-forcing receiver causes this gap to converge to a constant loss. The predictions of Table I are more clearly validated in this figure as the scenarios with a larger dimensionality deficit fall off quicker as the system progresses from a noise-limited regime to an interference-limited regime.

V. ROBUSTNESS TO LINK RANGE VARIATIONS

For opportunistic deployment, the link range may differ considerably from the nominal range R_o for which the transceiver apertures are designed (See Fig. 1). In particular, it is possible for columns of the channel matrix to become linearly dependent at certain ranges *smaller* than nominal, causing mode collapse and unacceptable noise enhancement due to interference suppression. In this section we discuss in detail how spatial oversampling with regularly spaced additional receive elements provides robustness to mode collapse as well as geometric misalignment. Analytical guidelines like the amount of spatial oversampling and the optimal choice of the additional receive element groups to circumvent mode collapse at non-optimal link ranges is presented for an *ideally aligned* system (4×4 LoS MIMO system with no geometric misalignment). We show that geometric misalignment of the panels does not help us while operating at varying link ranges and the guidelines presented for the ideally aligned system also work for misaligned systems, as long as the adaptive time window for space-time equalization is chosen based on the guidance of the previous section.

For the running example an ideally aligned system operating at a carrier frequency of 130 GHz at a link distance of $R_o = 100$ m is considered with the optimal inter-antenna spacing set based on the Rayleigh criterion [14], [22] as 34 cm to obtain a well-conditioned spatial channel. Table II lists the optimal element spacing based on this criterion for the considered LoS MIMO system with square arrays at different link range values. When the Rayleigh criterion is fulfilled, the channel matrix becomes scaled unitary, allowing for the recovery of the noisy transmitted signal through linear spatial equalization without degradation in the signal-to-noise ratio (SNR).

A. Spatial correlation between streams: Operating at ranges different from the nominal results in correlation between the columns of the LoS MIMO channel matrix, **H**. For an ideal $N \times N$ LoS MIMO system, the channel matrix with entries $\tilde{h}_{m,n}$ corresponding to the complex channel gain from the nth transmit element to the mth receive element is defined as

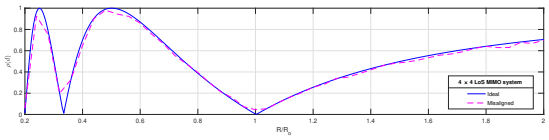

Fig. 8. Correlation among the columns of the channel matrix **H** as a function of link range for transmit elements separated by a distance d

$$\tilde{h}_{m,n} = e^{-j2\pi l(m,n)/\lambda} \tag{11}$$

where, $l(m,n)$ is the path length between the two above mentioned elements and λ is the corresponding carrier wavelength. Since only the relative phase shifts between the elements of **H** are of interest, the entries $\tilde{h}_{m,n}$ can be normalized by a factor of $e^{j2\pi R_o/\lambda}$ which results in the following form

$$h_{m,n} = e^{-j2\pi(l(m,n)-R_o)/\lambda} = e^{-j2\pi\Delta l(m,n)/\lambda} \tag{12}$$

where the differential distance $\Delta l(m,n)$ is equal to $l(m,n) - R_o$. If the coordinate location of the nth transmit element is x_n and the mth receive element is x_m, the path length difference (relative to R_o) for an inter-element spacing of d is

$$\Delta l(m,n) = \sqrt{(x_m - x_n)^2 + R_o^2} \approx (x_m - x_n)^2 \frac{d^2}{2R_o} \tag{13}$$

where $(x_m - x_n)d << R_o$. The entries of the channel matrix **H** is then given by

$$h_{m,n} \approx e^{-j(x_m-x_n)^2\pi d^2/(\lambda R_o)} = e^{-j(x_m-x_n)^2\psi} \tag{14}$$

where

$$\psi = \frac{\pi d^2}{\lambda R_o}. \tag{15}$$

When the operating link range R is not equal to the optimal link range, we can substitute for d using (2) to yield,

$$\psi = \frac{\pi}{2}\left(\frac{R_o}{R}\right) \tag{16}$$

For the ideally aligned system in consideration, the spatial correlation between the receive array responses to the kth transmit element and the nth transmit element with $k \neq n$ is given by [15]

$$\rho(k,n) = \frac{|\mathbf{h}_k^H \mathbf{h}_n|}{||\mathbf{h}_k||||\mathbf{h}_n||} \tag{17}$$

Fig. 8 plots the correlation $\rho(k,n)$ of the receive array responses to transmit elements k and n as the link range is varied from $R = 0.2R_o$ to $R = 2R_o$ for an ideally aligned system and its misaligned counterpart. We use the notation $\rho(d)$ to depict the normalized correlation among the receive responses to neighboring transmit elements i.e., transmit elements separated by a distance d. Using 14, this correlation in terms of the phase difference between the neighboring elements ψ can be expressed as

$$\rho(d) = \cos(\psi) \tag{18}$$

Similarly, the normalized correlation between the diagonal transmit elements, i.e., the transmit elements separated by a distance $\sqrt{2}d$ is denoted by $\rho(\sqrt{2}d)$, and can be expressed in terms of ψ as

$$\rho(\sqrt{2}d) = \cos^2(\psi) \tag{19}$$

The detailed derivation of the final forms presented in (18) and (19) is described in Appendix B. From Fig. 8, the correlation between two or more columns of $\mathbf{H}$ approach unity for certain values of link range R that leads to an ill-conditioned channel. It is observed that the columns of the channel matrix are almost entirely correlated at $R = 0.25R_o$ and $R = 0.5R_o$ as seen by the blue curve for the ideally aligned system. The high normalized correlation values between streams indicate the susceptibility of the system to suffer mode collapse while operating at these link range values. The misaligned system follows a similar trend to the ideally aligned system as indicated by the dotted curve in Fig. 8. It is important to recognize that the misaligned system is faced with some residual correlation even at $R = R_o$ validating our statement that geometric misalignment does not help our case when operating at varying link ranges. A similar analysis can be made for the normalized spatial correlation $\rho(\sqrt{2}d)$ for the ideally aligned and misaligned systems that has been excluded for brevity.

B. Effective Noise Enhancement: To explore the impact of spatial correlation on system performance, we study the resulting noise enhancement at the output of a zero-forcing (ZF) spatial equalizer. The ZF correlator is expressed as [23]:

$$\mathbf{C}_{ZF} = \mathbf{H}^{\dagger} = \mathbf{H}^{H}(\mathbf{H}\mathbf{H}^{H})^{-1} \tag{20}$$

Alternatively, the ZF correlator can be expressed as a scalar multiple of the projection of the desired signal stream (say $\mathbf{x}_1$) onto the interference subspace (spanned by $\mathbf{x}_2, \ldots, \mathbf{x}_N$). The fraction of signal energy lost as a consequence of this projection is equal to the inverse of the effective noise enhancement and is given as [24]

$$\frac{||\mathbf{P}_I^{\perp}\mathbf{x}_1||^2}{||\mathbf{x}_1||^2} = 1 - \frac{1}{||\mathbf{x}_1||^2}\boldsymbol{\rho}_I\mathbf{Q}_I^{-1}\boldsymbol{\rho}_I \tag{21}$$

where $\mathbf{P}_I^{\perp}\mathbf{x}_1$ is the projection of the desired signal orthogonal to the interference subspace, $\mathbf{Q}_I$ is the matrix of correlations between the interference vectors and $\boldsymbol{\rho}_I$ is the vector of correlations between the desired stream and the interference vectors. For the ideal 4×4 LoS MIMO system, $\boldsymbol{\rho}_I$ corresponding to desired stream $\mathbf{x}_1$ can be expressed in terms of $\rho(d)$ and $\rho(\sqrt{2}d)$ as

$$\boldsymbol{\rho}_I = \begin{pmatrix} \rho(d) \\ \rho(\sqrt{2}d) \\ \rho(d) \end{pmatrix} \tag{22}$$

and the interference correlation matrix $\mathbf{Q}_I$ is

$$\mathbf{Q}_I = \begin{pmatrix} 1 & \rho(d) & \rho(\sqrt{2}d) \\ \rho(d) & 1 & \rho(d) \\ \rho(\sqrt{2}d) & \rho(d) & 1 \end{pmatrix} \tag{23}$$

The effective noise enhancement is then found by computing the inverse of (21). For the ideally aligned system the noise enhancement at various link range values is plotted in Fig. 9. In our simulations, the calculated noise-enhancement values have been capped at 60 dB. A sharp increase in the noise enhancement is observed as soon as operating link range deviates from the optimal link range and, the overall noise enhancement is highest at $R_o = 0.25R$ and $R_o = 0.5R$. This behavior is consistent with the increased spatial correlation between the columns of the channel matrix for these values of R as seen in Fig. 8. The high noise enhancement values at a range R can be used as stand-in to predict the possible mode-collapse of the system and thus provides us with a single number value to predict the effectiveness of the system when operating at a range $R \neq R_o$.

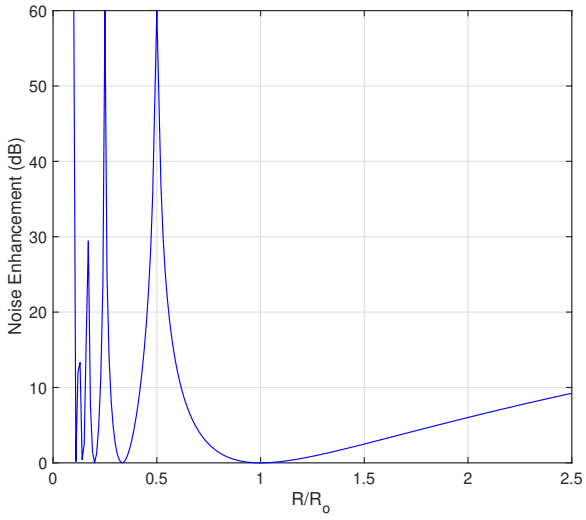

Fig. 9. Noise enhancement as a function of normalized link range for 4×4 LoS MIMO system

TABLE III
NORMALIZED CORRELATION BETWEEN STREAMS IN TERMS OF ψ

ρ	group 'b'	group 'c'	group 'd'
$\rho(d)$	$\cos(\psi/2)$	$\cos^2(\psi/2)$	$\cos^2(\psi/4)$
$\rho(\sqrt{2}d)$	$\cos^2(\psi/2)$	$\cos(\psi)$	$\cos(\psi/2)$

We can extend a similar analysis to the spatially oversampled system. As seen from Fig. 4, we induce $2\times$, $3\times$ and $4\times$ spatial oversampling at the receiver by adding additional receive elements in groups of 4 labelled 'a' to 'd' and placing them in a symmetric manner within the receive form-factor. Here, group 'a' corresponds to the base set of receive elements corresponding to an ideally aligned system with critical spatial sampling. The sequence in which we spatially oversample (e.g., selecting group 'c' instead of group 'b' to introduce a spatial oversampling factor of $2\times$) does not affect system performance under geometric misalignment. However, the effective correlation between streams is influenced by the geometry of the additional receive antennas as seen from (14). Therefore, it is crucial to answer the question: which

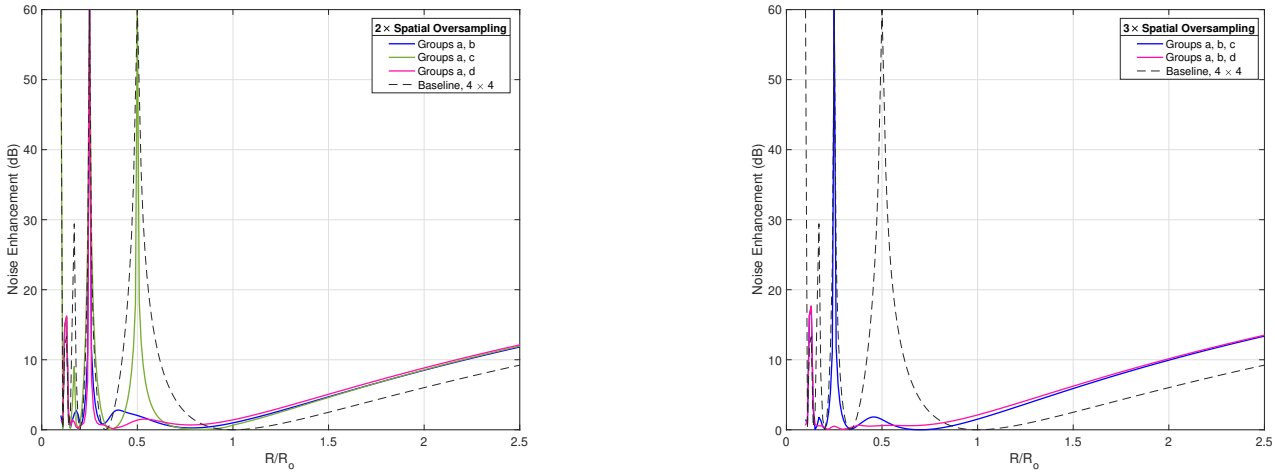

(a) (b)

Fig. 10. Noise enhancement as a function of range for the spatially oversampled system for different receive geometries for (a) $2\times$ and (b) $3\times$ spatial oversampling

configuration of receive antennas for a given spatial oversampling factor yields the lowest correlation between streams at a desired range of operation R? The normalized spatial correlation between streams can be calculated in a similar manner as the ideally aligned system in terms of ψ, for each of the the spatial oversampling groups described in Fig. 4. The resulting expressions for $\rho(d)$ and $\rho(\sqrt{2}d)$ as a cosine function of ψ are found in Table III. An example derivation of this form for group 'b' is provided in Appendix B. We can now utilize these groups as building blocks to curate an optimal receive geometry with the goal of minimizing the overall noise enhancement at a link range R for a given spatial oversampling factor. For example, a $2\times$ spatially oversampled system has three possible choices for the receive geometry starting with the base group 'a' as described in Fig. 4. Using Table III, the effective normalized spatial correlation for the choice of group 'b' is found as

$$\left.\begin{aligned}\rho_{ab}(d) &= (\cos(\psi)+\cos(\psi/2))/2\\ \rho_{ab}(\sqrt{2}d) &= (\cos(\psi)+\cos^2(\psi/2))/2\end{aligned}\right\} \quad (24)$$

In general, the expression for the normalized spatial correlation for a particular spatial oversampling factor and receiver configuration is built by summing up the corresponding expressions from Table III and diving the resulting expression by the spatial oversampling factor. The overall noise enhancement as a function of link range for the $2\times$ and $3\times$ spatially oversampled system corresponding to different receive geometries is plotted in Fig. 10(a) and Fig. 10(b) respectively. Some key design insights are as follows: 1) With sufficient spatial oversampling the peaks in noise enhancement seen in the ideally aligned system are significantly brought down. 2) For a given spatial oversampling factor, the choice of the receiver geometry becomes vital to ensure the lowest possible noise enhancement at a given link range. For example, with $2\times$ spatial oversampling, the receive geometry formed by the choice of Group 'a' followed by Group 'b' yields a lower noise enhancement compared to the choice of Group 'a' followed by Group 'c' at $R = 0.5R_o$ as seen in Fig. 10(a). Further, the lowest noise enhancement at $R = 0.5R_o$ with $N_{\text{rx}} = 8$ receivers is achieved with the receiver geometry choice of Group 'a' followed by Group 'd'. 3) From Fig. 10(a) it is apparent that none of the geometric receive element combinations with $N_{\text{rx}} = 8$ elements is sufficient to circumvent the high noise enhancement at $R = 0.25R_o$. However, with $3\times$ spatial oversampling and the right choice of receive geometry (picking Group 'd' over Group 'c'), the high noise enhancement is reduced, as seen in Fig. 10(b).

In order to understand the *cost* of operating at link distances $R \neq R_o$ with spatial oversampling, we define an effective link margin relative to an ideally aligned critically sampled link, as follows:

$$\begin{aligned}\text{Required Link Margin (dB)} = \text{Noise Enhancement at } R \text{ (dB)}\\ -10\log_{10}(N_{\text{rx}}/N_{\text{tx}}) + 20\log_{10}(R/R_o)\end{aligned} \quad (25)$$

where, $10\log_{10}(N_{\text{rx}}/N_{\text{tx}})$ is the receive beamforming gain in dB from spatially oversampling at the receiver and $10\log_{10}(R/R_o)$ is the propagation gain in dB from operating at a link distance R. We define this link margin solely as a means of quantifying the impact of range variations; link margins to account for other effects must be budgeted separately. At ranges smaller than nominal, we thus "get credit" for reduced propagation loss while dealing with fluctuations in the noise enhancement, while for ranges larger than nominal, we are penalized due to increases in propagation loss and noise enhancement. We plot this required link margin as a function

of the spatial oversampling factor and corresponding receiver geometry for various link ranges in Fig. 11, utilizing, for a given oversampling factor, the best geometries as determined from the results in Figs. 10(a) - 10(b). These results are shown to be consistent with the BER plots in Fig. 12, which shows BER versus SISO SNR for a selection of settings. The behavior for link ranges smaller than nominal ($R < R_o$) and larger than nominal ($R > R_o$) is qualitatively different:

- Drastic DoF collapse can happen at ranges smaller than nominal, and is alleviated by spatial oversampling. For the ideally aligned system without oversampling, there are significant peaks in noise enhancement (and hence required link margin) at ranges smaller than the nominal, specifically at $R = 0.5R_o$ and $R = 0.25R_o$. From Fig. 11, we see that $2\times$ spatial oversampling (8 receive antennas) removes the peak in required link margin at $R/R_o = 0.5$ but not at $R/R_o = 0.25$. Correspondingly, there is no error floor in Fig. 12 for $R/R_o = 0.5$, but there is an error floor for $R/R_o = 0.25$. $3\times$ oversampling (12 receive antennas) removes the peaks in required link margin at both $R/R_o = 0.5$ and $R/R_o = 0.25$. This is consistent with the absence of an error floor in Fig. 12 for$R/R_o = 0.25$.
- At link ranges greater than the nominal, the increase in required link margin is gradual, corresponding to gradual increases in propagation loss and noise enhancement (due to correlation between receive array responses for the different transmitted streams). For an ideally aligned system, spatial oversampling provides a gain due to noise averaging, but we do not see the full array gain because the noise enhancement also increases: at ranges larger than nominal, as we add more receive antennas, the normalized correlations between arrays responses for different streams also go up. This gain is reduced by the increased spatial correlation Thus, moderate levels ($2\times$ and $3\times$) of spatial oversampling offers limited benefits for ideally aligned systems at ranges larger than nominal. Of course, spatial oversampling remains crucial for geometrically misaligned links in these regimes as well.

Overall, for ranges smaller than nominal, spatial oversampling allows us to extend the regime without mode collapse. In this regime, the smaller propagation loss compensates for small fluctuations in noise enhancement, and we do not require any additional link margin relative to an ideally aligned, critically sampled link at nominal range. This holds, for example, for $2\times$ oversampling for $0.25 < R/R_o \leq 1$, and for $3\times$ oversampling for $0.13 < R/R_o \leq 1$. On the other hand, in order to operate at ranges larger than nominal, we do require additional link margin to compensate for the increased propagation loss and noise enhancement for the moderate levels of spatial oversampling that we consider, but a 10 dB link margin allows us to extend the range up to $R/R_o = 2.5$ for both $2\times$ and $3\times$ oversampling. In concrete numbers, if we are willing to expend 10 dB of link margin for range extension, the regime of robust operation for a 4×4 LoS

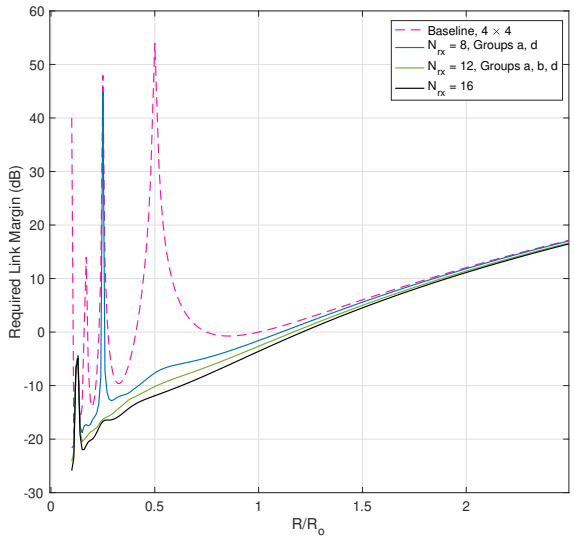

Fig. 11. Required link margin in dB as a function of link range for different spatial oversampling factors for the Ideal LoS MIMO system

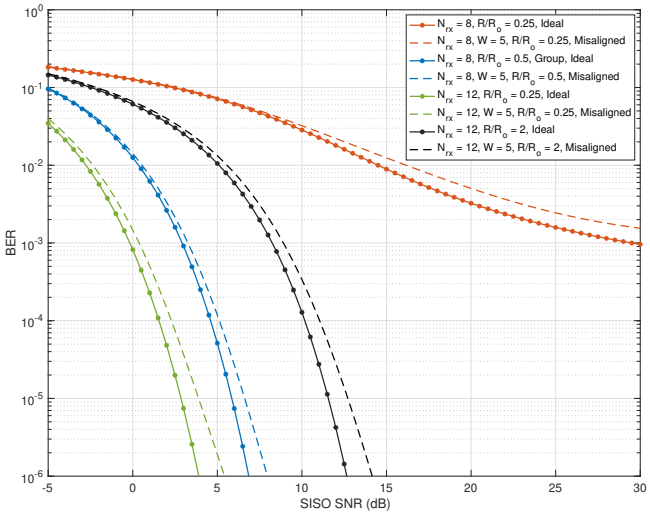

Fig. 12. BER Vs SISO SNR for spatially oversampled aligned and misaligned LoS MIMO at varying link ranges

MIMO link dimensioned for a nominal range of $R_o = 100$ m can be extended to 25 m $< R \leq 250$ m with $2\times$ spatial oversampling, and to 13 m $< R \leq 250$ m with $3\times$ oversampling. These design guidelines hold for geometrically misaligned links with the understanding that an appropriate adaptive space-time window, as designed in Section IV, is employed for equalization.

VI. Conclusion

Our work opens up the possibility of opportunistically deployed wireless networks with spatially multiplexed links, with spatial oversampling at the receiver providing robustness against both geometric misalignments and link range variations. We have shown that the intersymbol interference and

cross-stream interference caused by geometric misalignments can be overcome using a powerful combination of spatial oversampling combined with adaptive time windowing. Design rules for the required spatial oversampling factor and the temporal window size can be derived by simple signal space arguments, comparing the number of interference vectors against the dimension of the space-time equalizer. For instance, for our running example of 4 spatially multiplexed streams, a spatial oversampling factor of 2 (8 receive antennas) and a temporal window of 3 suffices to prevent error floors at high SNR, and for a spatial oversampling factor of 4 (16 receive antennas) a window size of 1 suffices.

Spatial oversampling with appropriately chosen receive elements also prevents DoF collapse when operating at link ranges different from the nominal range for which the transceiver apertures are dimensioned. We use the effective noise enhancement of the ZF spatial equalizer for an ideally aligned LoS MIMO system to design the spatial oversampling factor and the placement of additional receive elements. We then verify that such designs also provide robustness against mode collapse for geometrically misaligned links, provided that the adaptive time window of samples is chosen to be large enough for the ZF space-time equalizer to exist.

Simulation results for our system model (not included in this paper due to lack of space) show that spatial oversampling also reduces the required analog-to-digital converter (ADC) precision, consistent with results presented for simplified models in [25]. An interesting open problem is to understand the fundamental limits of required ADC precision as a function of constellation size in our setting. Another interesting direction for future work is to investigate the combination of transmit precoding with receive space-time equalization in order to reduce computational complexity and dynamic range requirements.

Appendix A
Link Budget Calculation

Link budget calculation for the 4×4 LoS MIMO system for square transceivers with 4 subarrays each at the transmitter and receiver respectively is detailed in this section. Each subarray at the transmitter contains N_t elements and each subarray at the receiver contains N_r elements. We evaluate the link budget for different subarray sizes with the following considerations:

- antenna element gian covering a hemisphere is 3 dBi
- a total transmit beamforming gain of $10\log_{10}(N_t)$ dB, plus a $10\log_{10}(N_t)$ dB power pooling gain is obtained from the N_t element subarray at the transmitter
- a total receive beamforming gain of $10\log_{10}(N_r)$ dB is obtained from the N_r element subarray at the receiver
- the noise figure of each RF chain is 7 dB
- the thermal noise of 30 GHz BW is about -71 dBm
- SNR of 10.2 dB is required for QPSK modulation
- link margin of 10 dB is desired
- a rain attenuation of 7 dB/Km which corresponds to a rain rate of 50mm/hr [26], [27] (moderate rainfall) is also included in the path loss calculation

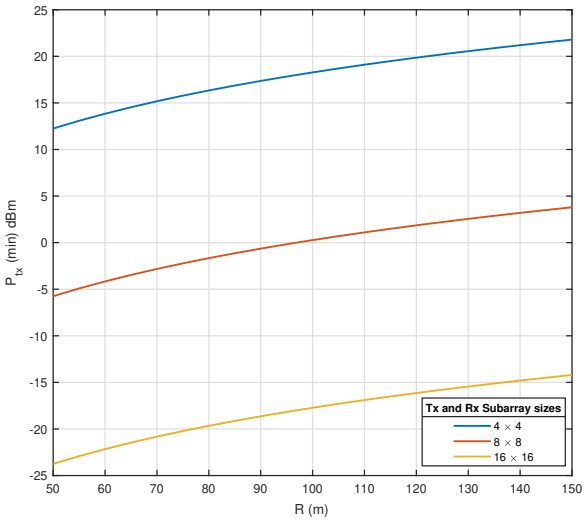

Fig. 13. Minimum required transmit power at varying link ranges and subarray sizes for the considered 4×4 LoS MIMO system with fixed inter-antenna spacing of 34 cm

We then obtain a receiver sensitivity of -54 dBm. Fig. 13 plots the minimum required transmit power at varying link ranges and subarray sizes for the considered system model with fixed transceiver form factors. From Fig. 13, for $R_o = 100$ m we require a minimum transmit power of 17 dBm with 16 element subarrays at both the transmitter and receiver. Additionally, without adjusting the transceiver form factors we see that only modest values for transmit power are required to operate even at non-optimal link ranges.

Appendix B
Spatial Correlation for Different Receiver Groups

In this section we aim to explicitly derive the forms described in Table III for some of the varying receive element groups shown in Fig. 4. The spatial correlation between streams is given as $\rho(d)$ and $\rho(\sqrt{2}d)$ can be expressed in terms of cosine functions of ψ using (14) for the four streams in the considered 4×4 LoS MIMO system.

A. Group 'a'

The effective phase difference experienced by the four receive elements 'a1' - 'a4' corresponding to different transmit streams is given as

$$\left.\begin{aligned} \mathbf{h}_1^T &= [1 \;\; e^{-j\psi} \;\; e^{-j2\psi} \;\; e^{-j\psi}] \\ \mathbf{h}_2^T &= [e^{-j\psi} \;\; 1 \;\; e^{-j\psi} \;\; e^{-j2\psi}] \\ \mathbf{h}_3^T &= [e^{-j2\psi} \;\; e^{-j\psi} \;\; 1 \;\; e^{-j\psi}] \end{aligned}\right\} \tag{26}$$

The normalized spatial correlation $\rho_a(d)$ is then calculated using (17) between $\mathbf{h}_1$ and $\mathbf{h}_2$ as

$$\rho_a(d) = (e^{j\psi} + e^{-j\psi} + e^{-j\psi} + e^{j\psi})/4 = \cos\psi \tag{27}$$

Similarly, $\rho_a(\sqrt{2}d)$ is calculated as the normalized correlation between $\mathbf{h}_1$ and $\mathbf{h}_3$ by antenna geometry as

$$\rho_a(\sqrt{2}d) = (e^{j2\psi} + 1 + e^{-j2\psi} + 1)/4 = \cos^2\psi \qquad (28)$$

B. Group 'b'

The effective phase difference seen across the receive elements 'b1'-'b4' is dependent on the receive geometry depicted in Fig. 4 and takes the following form

$$\left.\begin{aligned} \mathbf{h}_1^T &= [e^{-j\psi/8} \;\; e^{-j5\psi/8} \;\; e^{-j9\psi/8} \;\; e^{-j5\psi/8}] \\ \mathbf{h}_2^T &= [e^{-j5\psi/8} \;\; e^{-j\psi/8} \;\; e^{-j5\psi/8} \;\; e^{-j9\psi/8}] \\ \mathbf{h}_3^T &= [e^{-j9\psi/8} \;\; e^{-j5\psi/8} \;\; e^{-j\psi/8} \;\; e^{-j5\psi/8}] \end{aligned}\right\} \qquad (29)$$

Then, the normalized spatial correlation $\rho_b(d)$ is calculated in a similar manner to Group 'a' as

$$\rho_b(d) = (e^{j\psi/2}+e^{-j\psi/2}+e^{-j\psi/2}+e^{j\psi/2})/4 = \cos\psi/2 \quad (30)$$

It follows that $\rho_b(\sqrt{2}d)$ is then

$$\rho_b(\sqrt{2}d) = (e^{j\psi} + 1 + e^{-j\psi} + 1)/4 = \cos^2\psi/2 \qquad (31)$$

While the calculations for Group 'c' and Group 'd' have been excluded for the sake of brevity, it is easy to extend the same analysis across the other receive groups.

REFERENCES

[1] M. Sawaby, B. Grave, C. Jany, C. Chen, S. Kananian, P. Calascibetta, F. Gianesello, and A. Arbabian, "A fully integrated 32 Gbps 2x2 LoS MIMO wireless link with UWB analog processing for point-to-point backhaul applications," in *2020 IEEE Radio Frequency Integrated Circuits Symposium (RFIC)*, 2020, pp. 107–110.

[2] I. Sarris and A. R. Nix, "Design and performance assessment of high-capacity MIMO architectures in the presence of a line-of-sight component," *IEEE Transactions on Vehicular Technology*, vol. 56, no. 4, pp. 2194–2202, 2007.

[3] C. Sheldon, E. Torkildson, M. Seo, C. P. Yue, M. Rodwell, and U. Madhow, "Spatial multiplexing over a line-of-sight millimeter-wave mimo link: A two-channel hardware demonstration at 1.2gbps over 41m range," in *2008 European Conference on Wireless Technology*, 2008, pp. 198–201.

[4] F. Bohagen, P. Orten, and G. E. Oien, "Design of optimal high-rank line-of-sight MIMO channels," *IEEE Transactions on Wireless Communications*, vol. 6, no. 4, pp. 1420–1425, 2007.

[5] E. Torkildson, U. Madhow, and M. Rodwell, "Indoor millimeter wave MIMO: Feasibility and performance," *IEEE Transactions on Wireless Communications*, vol. 10, no. 12, pp. 4150–4160, Dec. 2011.

[6] J. F. Buckwalter, M. J. W. Rodwell, K. Ning, A. Ahmed, A. Arias-Purdue, J. Chien, E. O'Malley, and E. Lam, "Prospects for high-efficiency silicon and lll-v power amplifiers and transmitters in 100-300 ghz bands," in *2021 IEEE Custom Integrated Circuits Conference (CICC)*, April 2021, pp. 1–7.

[7] R. D. Gitlin and S. B. Weinstein, "Fractionally-spaced equalization: An improved digital transversal equalizer," *The Bell System Technical Journal*, vol. 60, no. 2, pp. 275–296, 1981.

[8] Proakis, *Digital Communications 5th Edition*. McGraw Hill, 2007.

[9] Ericsson Press Release, "Deutsche Telekom and Ericsson top 100Gbps over microwave link," May 2019. [Online]. Available: https://www.ericsson.com/en/press-releases/2019/5/deutsche-telekom-and-ericsson-top-100gbps-over-microwave-link

[10] T. Ingason, H. Liu, M. Coldrey, A. Wolfgang, and J. Hansryd, "Impact of frequency selective channels on a line-of-sight MIMO microwave radio link," in *2010 IEEE 71st Vehicular Technology Conference*, 2010, pp. 1–5.

[11] X. Song, D. Cvetkovski, W. Rave, E. Grass, and G. Fettweis, "Sequential channel equalization in strong line-of-sight MIMO communication," *IEEE Transactions on Wireless Communications*, vol. 18, no. 1, pp. 340–356, 2019.

[12] B. Mamandipoor, M. Sawaby, A. Arbabian, and U. Madhow, "Hardware-constrained signal processing for mm-Wave LoS MIMO," in *2015 49th Asilomar Conference on Signals, Systems and Computers*, 2015, pp. 1427–1431.

[13] P. Raviteja and U. Madhow, "Spatially oversampled demultiplexing in mmWave LoS MIMO," in *IEEE 19th International Workshop on Signal Processing Advances in Wireless Communications (SPAWC)*, June 2018, pp. 1–5.

[14] F. Bøhagen, P. Orten, and G. Øien, "Optimal design of uniform rectangular antenna arrays for strong line-of-sight mimo channels," *Journal of Wireless Communications and Networking*, vol. 2007, p. 045084, 2007. [Online]. Available: https://doi.org/10.1155/2007/45084

[15] E. Torkildson, C. Sheldon, U. Madhow, and M. Rodwell, "Nonuniform array design for robust millimeter-wave mimo links," in *Proceedings of the 28th IEEE Conference on Global Telecommunications*, ser. GLOBECOM'09. IEEE Press, 2009, p. 4826–4832.

[16] L. Zhou and Y. Ohashi, "Design of non-uniform antenna arrays for robust millimeter-wave los mimo communications," in *2013 IEEE 24th Annual International Symposium on Personal, Indoor, and Mobile Radio Communications (PIMRC)*, 2013, pp. 1397–1401.

[17] M. Tawada, Y. Ohta, and A. Nagate, "Design of robust los-mimo transmission in haps feeder link," in *2022 IEEE 96th Vehicular Technology Conference (VTC2022-Fall)*, 2022, pp. 1–7.

[18] N. Matsumura, K. Nishimori, R. Taniguchi, T. Hiraguri, T. Tomura, and J. Hirokawa, "Novel unmanned aerial vehicle-based line-of-sight mimo configuration independent of transmitted distance using millimeter wave," *IEEE Access*, vol. 8, pp. 11 679–11 691, 2020.

[19] M. H. Castañeda Garcia, M. Iwanow, and R. A. Stirling-Gallacher, "Los mimo design based on multiple optimum antenna separations," in *2018 IEEE 88th Vehicular Technology Conference (VTC-Fall)*, 2018, pp. 1–5.

[20] L. Giridhar, M. E. Rasekh, A. D. Sezer, and U. Madhow, "Adaptive space-time equalization with spatial oversampling for misaligned los mimo," in *2022 IEEE Wireless Communications and Networking Conference (WCNC)*, 2022, pp. 1569–1574.

[21] U. Madhow, *Introduction to Communication Systems*. Cambridge University Press, 2014.

[22] P. Larsson, "Lattice array receiver and sender for spatially orthonormal mimo communication," in *2005 IEEE 61st Vehicular Technology Conference*, vol. 1, 2005, pp. 192–196 Vol. 1.

[23] U. Madhow, *Fundamentals of Digital Communication*. Cambridge University Press, 2008.

[24] U. Madhow and M. Honig, "Mmse interference suppression for direct-sequence spread-spectrum cdma," *IEEE Transactions on Communications*, vol. 42, no. 12, pp. 3178–3188, 1994.

[25] A. D. Sezer, U. Madhow, and M. J. W. Rodwell, "Spatial oversampling for quantized los mimo," in *2021 55th Asilomar Conference on Signals, Systems, and Computers*, 2021, pp. 405–409.

[26] N. Al-Falahy and O. Y. K. Alani, "Design considerations of ultra dense 5g network in millimetre wave band," in *2017 Ninth International Conference on Ubiquitous and Future Networks (ICUFN)*, 2017, pp. 141–146.

[27] Y. Karasawa and Y. Maekawa, "Ka-band earth-space propagation research in japan," *Proceedings of the IEEE*, vol. 85, no. 6, pp. 821–842, 1997.